Experimental setup for probing electron-induced chemistry in liquid micro-jets

OPEN ACCESS
IOP Publishing
Journal of Physics B: Atomic, Molecular and Optical Physics
J. Phys. B: At. Mol. Opt. Phys. **56** (2023) 215201 (7pp)
https://doi.org/10.1088/1361-6455/ad0205

Experimental setup for probing electron-induced chemistry in liquid micro-jets

Pamir Nag*, Miloš Ranković*, H Christian Schewe, Jozef Rakovský, Leo Sala, Jaroslav Kočišek and Juraj Fedor*

J. Heyrovský Institute of Physical Chemistry, Czech Academy of Sciences, Dolejškova 3, 182 23 Prague, Czech Republic

E-mail: pamir.nag@jh-inst.cas.cz, milos.rankovic@jh-inst.cas.cz and juraj.fedor@jh-inst.cas.cz

Received 5 June 2023, revised 3 October 2023
Accepted for publication 10 October 2023
Published 19 October 2023

Abstract

We present an experimental setup for probing chemical changes in liquids induced by electron collisions. The setup utilizes a custom-designed electron gun that irradiates a liquid microjet with an electron beam of tunable energy. Products of the electron-induced reactions are analyzed *ex-situ*. The microjet system enables re-circulation of the liquid and thus multiple irradiation of the same sample. As a proof-of-principle experiment, an aqueous solution of TRIS (2-Amino-2-(hydroxymethyl)propane-1,3-diol) was irradiated by 300 eV electron beam. Optical UV–VIS analysis shows that the electron impact on the liquid surface leads to the production of OH radicals in the solution which are efficiently scavenged by TRIS.

Keywords: liquid micro-jet, electron-induced chemistry, electron collisions

(Some figures may appear in colour only in the online journal)

1. Introduction

In the collision community, the term *electron-induced chemistry* is typically understood as changes in the structure of molecules upon their interaction with free (ballistic) electrons [1]. A number of elementary processes can trigger such chemical changes: dissociative ionization, dissociative electron attachment, or neutral dissociation (which starts with a vertical electronic excitation). The cross sections for these initial reactions strongly depend on the energy of incident electrons: the dissociative electron attachment is a resonant process typically operative in the energy range of up to 10 eV, while the ionization and excitation peak around 100 eV electron energy and then slowly drop down to keV region (where other processes such as core-excitation open up). The outcome of chemical reactions is thus sensitive to the energy of ballistic electrons. There are in principle two experimental approaches to probe such electron-induced chemistry: (i) those where the reactions are induced by an electron beam with well-defined energy and (ii) those where a broad distribution of electrons is present, e.g. plasma or high-energy irradiation experiments (where electrons are produced as secondary electrons).

Probing interactions with a well-defined electron beam is straightforward in experiments that probe samples in the form of molecular beams in a vacuum [1, 2]. Products of such electron-molecule (or electron-cluster) reactions are typically analyzed by mass spectrometry or by various imaging methods. A lot of attention has also been dedicated to probing the electron-induced chemistry in the solid-state samples which are typically cryogenically frozen on a solid substrate [3]. The reaction products in a solid state are either monitored *in situ*, by various surface-science techniques, or the samples

* Authors to whom any correspondence should be addressed.

are removed from the vacuum and analyzed by analytical methods [4].

A common denominator in all the above-mentioned experimental methods is that the samples are compatible with high vacuum and thus can be irradiated by a controlled electron beam. This is generally not the case with samples that are volatile liquids, e.g. aqueous solutions. A liquid's vapor pressure usually destroys the vacuum. Probing electron-induced chemistry in liquids has thus been limited to experiments where the electrons are created directly in the sample as secondary particles, e.g. various pulsed-radiolysis methods. These can be performed in a pump-probe manner and thus provide information about the ultrafast dynamics, however, control over the kinetic energy of electrons, inducing chemical reactions, is usually lacking in such experiments.

The liquid microjet technique has overcome the difficulty of introducing volatile liquids into the vacuum. Originally, it has been developed to study the evaporation processes of liquids in vacuum [5–7]. Nowadays, it is used in many fields of research concerning liquid-phase phenomena, namely any kind of x-ray absorption [8] and photo-electron spectroscopy [9, 10] microjets have also been used as targets for molecular collisions [11, 12] and collisions with fast ions [13]. An extension of the microjet technique, flat jet [8, 14], has been used in, e.g. high-harmonic generation [15], in imaging diffusion controlled chemical luminescence reactions [16], or in molecular beam scattering experiments [17].

In this paper, we present a new experimental setup in which an electron beam interacts with a liquid microjet. To our knowledge, the only previous setup combining electrons and microjets is that of Tian and co-workers [18, 19] which monitors ions created at the interface by a time-of-flight technique. The prospects of extracting collision cross sections from electron-microjet scattering have been explored by Muccignat *et al* [20] We are interested in chemical changes which are induced by electron impact in the liquid itself. We have developed a setup that enables recirculating of the liquid samples for multiple irradiations by electrons. The samples are then analyzed offline by standard chemical analysis techniques. We also present the first results on the electron-induced transformation of an aqueous solution of tris(hydroxymethyl)aminomethane (TRIS).

2. Effect of the gas-phase molecules evaporated from the microjet

The first issue which should be considered when judging the prospects of electron beam interactions with a liquid jet surface is the transmission of electrons through the cloud of evaporated molecules surrounding the jet. The scattering of electrons on the gas phase molecules could in principle lead to a strong attenuation of the incident beam.

To estimate this effect, we consider a microjet of pure H_2O with a radius R_{jet}. The density of the gas-phase molecules depends on the distance r from the jet center. Due to cylindrical symmetry this dependence can be approximated as

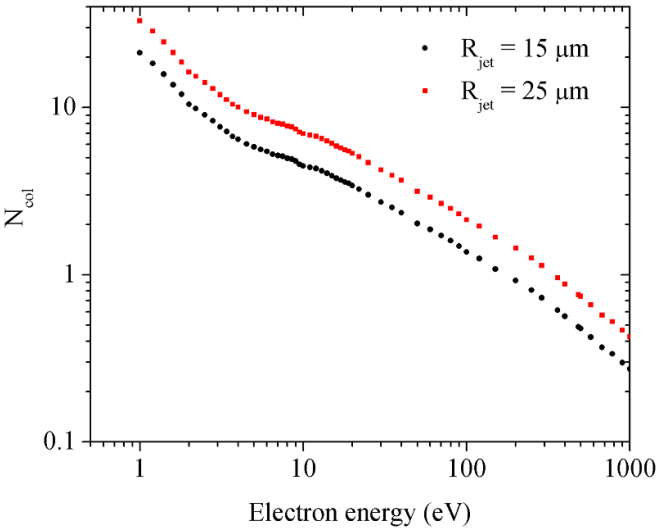

Figure 1. Average number of collisions N_{col} which the electron statistically undergoes on the way to the microjet according to equation (1) for $R_{gun} = 4$ cm and n_0 corresponding to local pressure of 6.1 mbar.

$n(r) = n_0 \frac{R_{jet}}{r}$ where n_0 is the gas number density at the surface. The electron with energy ε approaching the jet from a distance R_{gun} (e.g. the distance between the jet and the exit hole of a differentially pumped electron gun) will statistically undergo N_{col} collisions with gas-phase H_2O molecules:

$$N_{col}(\varepsilon) = \int_{R_{jet}}^{R_{gun}} n(r)\,\sigma(\varepsilon)\,\mathrm{d}r = n_0\sigma(\varepsilon)\,R_{jet}\ln\frac{R_{gun}}{R_{jet}}. \quad (1)$$

Here, $\sigma(\varepsilon)$ is the cross section for electron-H_2O collisions. We approximate it by the total scattering cross-section recommended by Itikawa and Mason [21], other recommended cross sections [22, 23] yield very similar results.

Figure 1 shows the $N_{col}(\varepsilon)$ as obtained from equation (1) assuming n_0 corresponding to the saturated vapor pressure of 6.1 mbar [24] and $R_{gun} = 4$ cm, for two different jet radii. The total e-H_2O scattering is a strongly varying function of the electron energy and so is the resulting number of collisions. The electron will undergo on average less than one gas-phase collision for energies larger than approximately 100 eV (for the jet of 30 μm diameter) or 300 eV (for the jet of 50 μm diameter).

It should be noted that there is an inherent uncertainty in this simple model. It mainly concerns the value of n_0, the gas density at the water interface. The saturated vapor pressure is a sensitive function of water temperature. Due to evaporative cooling, the temperature of the jet decreases with the increasing downstream distance from the nozzle. The value of 6.1 mbar corresponds to water at 272 K and is the same as was used in similar numerical estimates by Faubel and co-workers [9, 24]. At 292 K, the vapor pressure of water is 23.4 mbar. Using n_0 corresponding to such pressure would increase N_{col} by a factor of 3.6 compared to that plotted in figure 1. The saturated vapor pressure approximation might be, however, an inappropriate representation of n_0 at a liquid

microjet surface: the apparent surface temperature determined from measurements of the velocity distribution of evaporated molecules is much lower than the freezing point of water—below 240 K [24]. It is likely that the evaporation from the jet is probably far from equilibrium [7]. The lower apparent temperature means lower n_0 and it would correspondingly lower the N_{col}. In spite of the uncertainty in the n_0 determination, the dominant factor for N_{col} is a strong dependence of $\sigma(\varepsilon)$ on the electron energy ε.

This fact guided the design of the present setup. Even though the collisions of low-energy electrons (e.g., below 10 eV) would be attractive since they could enable the direct formation of electronic resonances or a selective population of optically-forbidden electronic states in liquids, such slow electrons would not get to the surface through the vapor layer (at least in case of water and aqueous solutions). We will thus use incident energies higher than 100 eV. Even though such electrons can lead to a number of secondary processes in water and we thus need to compromise the aspect of chemical control by fine-tuning the incident electron energy, a high incident energy is necessary to reach the liquid surface.

3. Experimental setup

3.1. Overview

The setup consists of three vacuum chambers: (i) interaction chamber, (ii) cold trap chamber, and (iii) electron gun chamber. The overall scheme is shown in figure 2. A photograph of the interaction chamber is shown in figure 3.

In detail: the interaction chamber is a cubical vacuum chamber (203 mm side length) with six CF160 ports. It is located at the center of the setup. A turbo molecular pump with a pumping speed of 685 l/s for N_2 (Pfeiffer HiPace 700) is mounted from the top. It is backed by a scroll pump (Leybold Scrollvac 15 plus).

The electron gun chamber is a cross (279 mm in length) with two CF160 ports and two CF40 ports. The chamber is differentially pumped by a small turbo molecular pump with a pumping speed of 67 l/s for N_2 (Pfeiffer HiPace 80), mounted from the top and backed by a dry multi-stage root pump (Adixen ACP 15).

Another cross chamber (273 mm in length), with two CF160 ports and two CF100 ports, is connected to the interaction chamber. Two liquid nitrogen (LN_2) traps were mounted on this chamber to freeze the residual liquid vapor inside the interaction chamber to obtain a better vacuum. It turned out that the operation of only one LN_2 trap is sufficient, using the second one did not improve the background pressure during the jet operation.

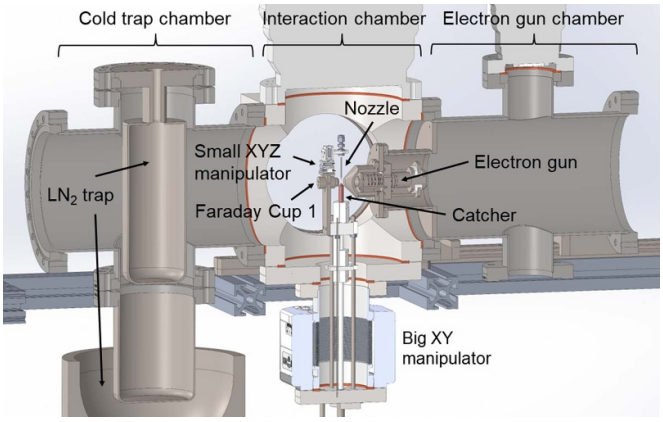

Figure 2. 3D model of the reactivity experimental setup.

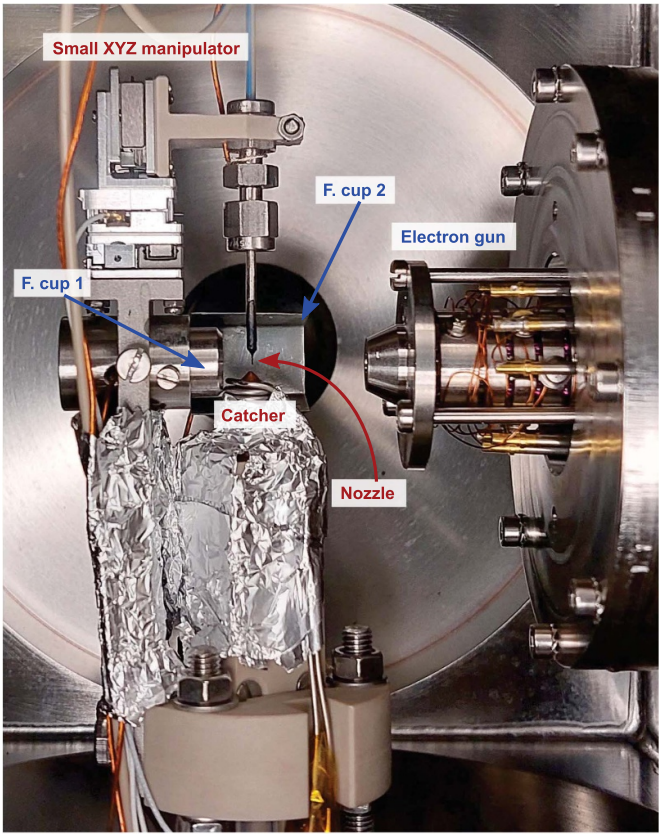

Figure 3. Photograph of the interaction chamber. A few electrodes from the low vacuum section of the electron gun are visible on the right side. The Faraday Cup 1 is used to measure the current of the primary electron beam, while the plate behind the Nozzle labeled as Faraday Cup 2 is used to measure the current of electrons that are scattered from the liquid jet. Graphite paint is used to cover the quartz glass Nozzle in order to minimize charging.

3.2. Electron gun and electronics

We designed and built a non-monochromated electron gun based on an earlier design by Milosavljević *et al* [25], with a number of modifications that will be described in this section. The scheme of the electron gun, together with the electron trajectories simulated in SIMION8.1, is shown in figure 4.

The cylindrical electrodes in the gun are made from 316 stainless steel and the insulating parts are made from machineable ceramics. The electrode spacings and alignment are done with rubidium balls of 1.5 mm and 2 mm diameters. The main difference from the original design is that we used an ES-526 Yttria-coated Iridium disc from Kimball Physics, specially optimized for increased electron emission in harsh

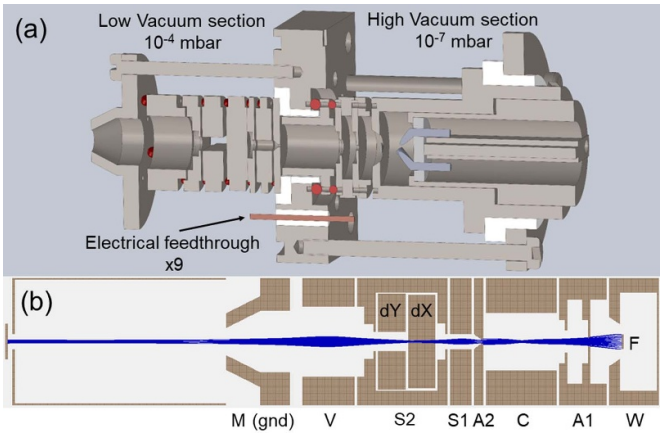

Figure 4. Cross-section of an electron gun: (a) stainless steel electrodes (gray), copper electrical feed-throughs (brown), rubby balls (red) and ceramic insulators (white), (b) electron beam trace (blue) obtained in SIMION8.1 for 600 eV electron energy. Electrode description: W—Wehnelt electrode; A1, A2—anode (extractors); C—1st focus, S1—2nd focus, S2—deflector unit; dX, dY—flat deflectors; V—final (3rd) focus, M—ground. Differential pumping is established via 0.5 mm aperture with a conical opening in electrode A2.

vacuum conditions. Other modifications include 2-axis flat deflector electrodes and the addition of a 2nd focusing electrode S1 before deflectors, for triple focusing. Moreover, we reduced the overall dimensions and changed the aspect ratios of all electrodes, and implemented a two-stage vacuum section with electrical feed-throughs to accommodate the differential pumping requirements. The latter is for keeping an electron source in the best possible vacuum conditions, in order to ensure a long lifetime.

We have also designed and built a microcontroller-based high-voltage electronics power supply to fully operate the electron gun remotely via a serial RS232 port communication with a PC. For data acquisition and electron gun control, we used a PC software called ELS (electron spectrometer processor), originally written by Allan [26]. We upgraded ELS with new modules and serial routines to facilitate the automatic tuning of all electrodes, scanning of electron energy and deflector positions, as well as the recording of the electron beam current in the Faraday Cup 1 and 2 using a Keithley 6485 picoampermeter. The gun's effective operating energy range is (100–700) eV. It should be noted that the electron gun is not shielded electrostatically or magnetically since it was designed to operate at energies above 100 eV, where we do not expect any major issues due to small constant residual electric or magnetic fields in the interaction chamber.

As recommended by Kimball Physics the filament power supply was operated in a constant voltage mode, while we kept the filament current relatively low around 3.7 A to ensure lower initial electron energy spread caused by thermal emission. By using a separate setup we measured the elastically scattered electrons from a water micro-jet and perform the energy calibration of the electron gun and measure the energy resolution. The measured energy resolution at full width at half maximum (FWHM) of the elastic peak is about 400 meV at 600 eV incident electron energy. The absolute energy scale uncertainty is of ± 0.5 eV in the full operating range. At 600 eV electron energy, the estimated focused beam spot size from simulation in SIMION at a focal distance of Faraday Cup 1, or 30 mm from the last electrode M (ground), is about 1 mm. This value is in good agreement with an experimentally obtained electron beam profile measured by the perpendicular movement of a Faraday Cup 1 across the electron beam. It should be noted that the distance of the liquid-jet nozzle is 17 mm from the electrode M and the optimal voltage for a focusing electrode V is selected in the optimization procedure as described in section 3.5.

3.3. Recirculating liquid microjet

The main component of the setup is the high-vacuum compatible recirculating liquid micro-jet system. Its schematic diagram is shown in figure 5. The liquid micro-jet is produced by passing the desired liquid sample at high pressure through a nozzle kept inside the vacuum chamber. The liquid jet is exposed to vacuum (background pressure in the range of 10^{-5} mbar with the jet) on a 3–5 mm length (adjustable by an XYZ-positioning stage described below), captured by a catcher unit and ultimately collected in a glass sample collector bottle kept outside of the vacuum chamber. It is possible either to reuse the collected sample for repeating the irradiation or to perform an *ex-situ* analysis of the sample. During these experiments, nozzles with either 30 or 50 μm inner diameter were used. The nozzles were prepared in-house by cutting fused silica capillaries with the chosen inner diameter and 150-micron outer diameter into about 5–7 mm length and then glueing with epoxy to a metallic pipe (either stainless steel or titanium) with a 1/16 inch outer and 200-micron inner diameters.

In the current configuration, it is possible to switch between up to four different solvent samples during the experiment with the help of a solvent selector. The liquid samples are kept at atmospheric pressure either at room temperature or in a cold bath depending on the stability of the sample. The liquid samples are passed through a vacuum degassing unit (DeltaChrom, model VD 060) to remove any solvated gas from the liquid and then connected to a four-channel sample selector unit. The output of the sample selector is connected with a high-performance liquid chromatography (HPLC) pump (Watrex P102). The outlet of the HPLC pump is connected with the nozzle using 1/16 inch outer diameter PEEK tubing. The nozzle is mounted on a vacuum-compatible triaxial positioning stage (Mechonics MS15 xyz-mounted, vacuum edition, denoted as 'Small XYZ manipulator' in figures 2 and 3) inside the vacuum chamber.

To collect the liquid jet after the electron beam irradiation, a copper catcher with a 1/4 inch outer diameter, around 20 mm length, and a conical-shaped top part with a 500-micron opening is placed 3–6 mm downstream from the nozzle. During the experiments, the catcher is heated between 55° and 75°C to prevent the freezing of the liquid. The copper catcher is connected with a 1/4 inch PEEK tube which ultimately leads outside of the vacuum chamber. The PEEK tube is connected to

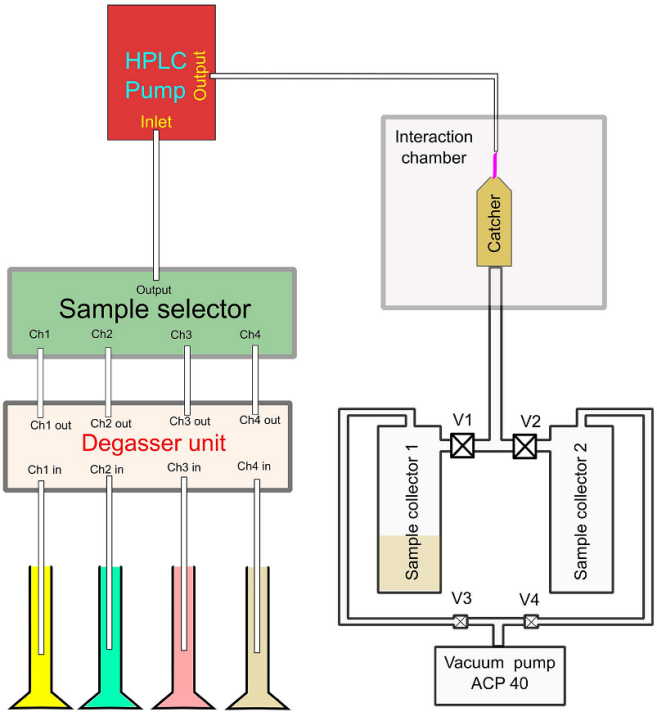

Figure 5. Schematic diagram of the recirculating liquid micro-jet production unit.

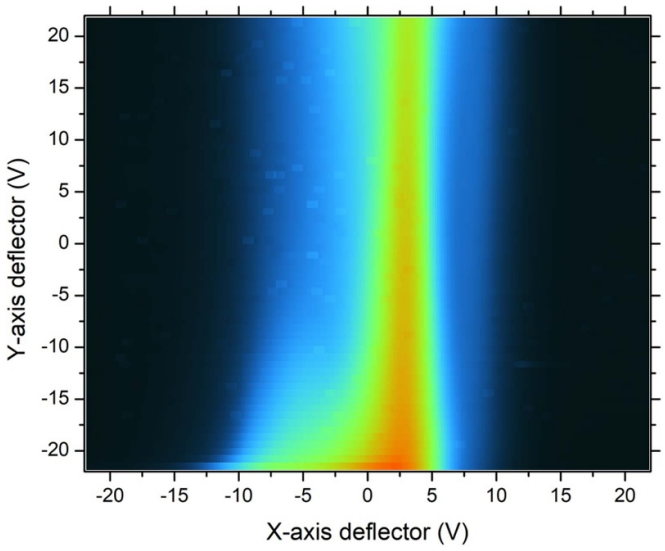

Figure 6. The electron scattering map as a function of the vertical and horizontal deflection of the incident electron beam, obtained in the Faraday Cup 2 at 600 eV energy for 1-propanol in the liquid microjet.

a glass sample collector bottle. A rough vacuum in the range of 2×10^{-1}–1 mbar is maintained inside the glass bottle using a multi-stage root pump, specially designed to pump water vapor (Adixen ACP 40CV).

The Nozzle, Catcher unit, Faraday Cup units 1 and 2, along with all electrical feedthroughs are mounted on a linear translation X,Y-manipulator (UHV Design Ltd XY aligner with +/- 10 mm of X and Y motion, denoted as 'Big XY manipulator' in figure 2) using a custom-made CF63 port so that the entire liquid jet assembly can be moved with respect to the incident electron beam. The liquid jet is produced by flowing the liquid sample with 0.75 ml min^{-1} to 1.2 ml min^{-1} flow rate depending on the property of the liquid. A pressure of around 65–110 bar is required in the nozzle tubing depending on the flow rate and the liquid. It was observed that it is important to maintain a minimum flow rate and a minimum pressure in the nozzle tubing to have a working jet and efficient collection system. If the flow rate is too low then the liquid starts flowing from the catcher unit back to the interaction region where it ultimately freezes. For the present configuration, it was observed that with pure water at least a flow rate of 0.65 ml min^{-1} is required to prevent the backflow of the liquid. Keeping the liquid jet and collection unit running is intricate and depends on the physical properties of the liquid in interest. The liquid jet and the recirculating system can be started on and stopped in a high vacuum (the background pressure before turning on the jet is in the 10^{-8} mbar range) with a 1-propanol sample. However, it is not possible to start the liquid jet with water in a high vacuum. During the present experiments, the liquid jet was always started in a high vacuum with 1-propanol and later switched to the sample of interest. Before stopping the jet, it was always switched to 1-propanol. On the collection unit side, it is possible to switch between two different collection bottles without breaking the continuity of the experiment. In this way, it is possible to reuse the collected sample or to perform an *ex-situ* analysis of the collected sample while the experiment is still running. It is also possible to switch between different samples or different experimental conditions and to collect the different sample products separately without having to stop the experiments in between.

3.4. Sample analysis

For the current experiments, an *ex-situ* UV–VIS spectrophotometer from Shimadzu (Model UV-1800) was used. The spectrophotometer is capable of measuring photo-absorption in the wavelength range from 190 nm to 1100 nm.

3.5. Optimization of the setup

To optimize the setup we monitored the scattered electrons from the liquid jet using a molybdenum plate, hereafter denoted as Faraday Cup 2. It is placed inside the vacuum chamber in a mutually perpendicular direction with respect to both the liquid jet and the electron beam direction. The Faraday Cup 2 was kept at 27 V floating potential using batteries to measure the current of the scattered electrons using a Keithley 6485 picoampermeter. The incident electron beam is scanned using the deflectors along the horizontal and vertical directions and the scattered electron current is measured on the Faraday cup 2. The 2D map of the scattered electron current, measured in Faraday Cup 2, as a function of the deflection voltages is shown in figure 6. The voltage on the focusing electrode V was adjusted to obtain the sharpest 2D map image.

The primary electron current measured in the Faraday Cup 1 can be set from a few pA to hundreds of nA by adjusting the

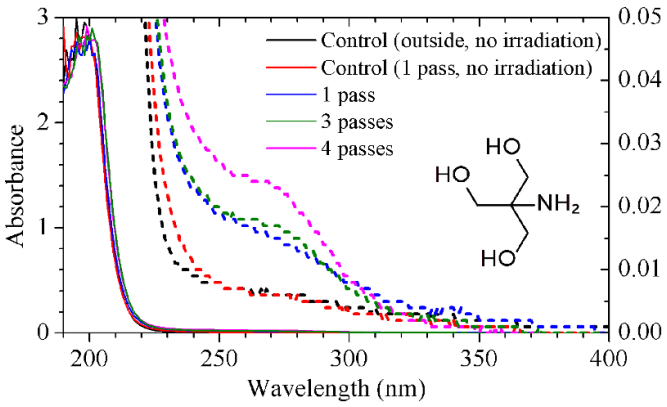

Figure 7. UV–VIS spectra of different samples. The solid lines show absorbance data (left vertical axis), the dashed lines are the same data in a magnified scale (right vertical axis). Details about the individual datasets are provided in the text.

filament current. During the present experiments, it was kept at around 10 nA in order to minimize electron beam instability and other issues due to charging and pressure variation with the liquid jet being started/stopped in a vacuum.

4. Results: electron-induced chemistry in aqueous solutions of TRIS

In the pilot experiments, we probed the electron irradiation of the aqueous solution of TRIS, $(HOCH_2)_3CNH_2$, 2-Amino-2-(hydroxymethyl)propane-1,3-diol (the structure is shown in the inset of figure 7). TRIS is one of the most common buffers in the biology/biochemistry laboratory practice (buffer solutions are used as a means of keeping pH at a nearly constant value, and the buffer range for TRIS, pH 7-9, coincides with the physiological pH typical of most living organisms). Additionally, TRIS is an effective OH radical scavenger [27, 28] and it efficiently protects DNA from high linear-energy transfer radiation [27]. It is thus used, for example, as a stabilizer in plasmid-DNA experiments.

Recently, Roush *et al* [29] suggested that TRIS can be used as an intrinsic hydroxyl radical dosimeter. They induced oxidation by the exposure of the aqueous solutions of TRIS with hydrogen peroxide to a pulsed KrF excimer laser and measured the ultraviolet absorbance of the irradiated samples. The laser irradiation caused a substantial absorbance increase in the wavelength region from 250 to 310 nm where a new band appeared with a maximum of around 265 nm (figure S1 in [29]). The band was attributed to a rather complex chemical reaction of TRIS with OH radicals produced from the H_2O_2 photolysis (figure S3 in [29]). This work inspired us to probe the transformation of TRIS solutions with electron impact.

The TRIS sample, solid at room temperature, was commercially purchased from Sigma-Aldrich with a stated purity of 99.9%. The current experiments were performed with a 19.7 mM solution of TRIS in water. The solution is then passed through the liquid microjet into the reaction chamber where it was irradiated with an electron beam of 300 eV incident energy.

Figure 7 shows the UV–VIS spectra. The 'Control (Outside, no irradiation)' is the sample of the solution which was left on the table. 'Control (1 pass, no irradiation)' is the sample that was passed through the liquid microjet setup with the filament on, however, with the electron beam blocked by one of the electron gun lenses (zero electron beam current obtained on the Faraday Cup). This sample probes a possible effect of photon-induced chemistry due to light from the filament, thermal chemistry, or any other effects caused by running the solution through the microjet system. Finally, samples '1 pass', '3 passes' and '4 passes' denote how many time the samples were passed through the microjet system while being irradiated by a 300 eV electron beam. The average electron beam current measured on the Faraday cup was about 5 nA.

The main absorbance peak of the pure TRIS aqueous solution is at 200 nm [29]. Upon electron irradiation, a weak but clearly distinguishable new band appears in figure 7 with a maximum of around 270 nm. This is in perfect agreement with the findings of Roush *et al* [29] who attributed this band to the reaction of TRIS with OH radicals. Therefore, we conclude that electrons are able to reach the liquid surface. Upon their interaction with the water solvent, OH radicals are formed and then scavenged by TRIS molecules.

Clearly, the intensity of the 270 nm band does not grow linearly with the number of passes through the jet. Several effects can influence the final concentration of the TRIS+OH product. First, the UV–VIS analysis is performed offline, where all the samples are first collected and then sent for analysis (the spectrometer is located in a different laboratory than the microjet setup). Second, the concentration of TRIS in the solution itself is not constant: upon passing through a vacuum, the jet evaporates. The vast majority of the evaporated molecules are water molecules and the concentration of TRIS thus increases with the number of passes through the vacuum. We estimated this increase from the value of absorbance at 210 nm (the absorbance was first calibrated with test solutions of increasing TRIS concentration which were analyzed on the same UV–VIS spectrometer). While the initial concentration of TRIS solution was 19.7 mM, after 1 pass it was 20.4 mM, while after 4 passes it reached 24.7 mM. Further effects related to the concentration of the irradiation products can be related to e.g. incomplete mixing of the solution when reintroducing the collected irradiated sample to the reservoir to complete the desired number of passes. Also in each pass, only the interfacial layer is irradiated.

The data shown in figure 7 are from one measurement run. We repeated this experiment three times at slightly different conditions (various TRIS concentrations and electron currents) with the same results (the band at 270 nm was growing, however, this growth did not show a linear dependence on the number of passes).

5. Conclusions

In conclusion, we present here a setup for analyzing macroscopic reactions induced in liquid samples by the impact of an electron beam with a well-defined energy. The setup combines

the liquid microjet nozzle with a catcher system which enables multiple irradiation passes of the same sample. The irradiation is performed using a custom-designed high-energy electron gun. The proof-of-principle experiment with the aqueous solutions of TRIS unambiguously shows that 300 eV electrons interact with the liquid surface and induce chemical changes that are macroscopically detectable by an offline UV–VIS analysis.

The setup can be in principle viewed as an extension of the increasingly used continuous-flow technology in organic synthesis [30, 31]. This extension can open up new avenues especially in electron-induced chemistry and electron catalysis. For example, it can be used to probe reactions which have a known outcome when they are induced by a photon absorption. For this purpose, the reaction chamber will be further equipped with light sources to enable comparison between photo-induced transformation versus electron impact induced ones. A specific example of such elementary reaction can be a cis-trans isomerization [32] or analogues of photo-redox reactions [33]. Electron impact can directly excite long-lived excited states which are optically spin-forbidden. The setup thus enables to explore the concept of triplet-state initiated chemistry, which can essentially be applied to any photochemical reaction involving triplet states.

Nevertheless, we must mention about a few limitations of the setup in current configuration. It is not possible to do experiments with liquids having high viscosity as it results too much pressure (more than 250 bar) behind the nozzle to achieve workable flow rate. Also it is difficult to recirculate liquids having significantly higher vapor pressure, for example pure methanol. We are trying to gain more experience and improve the setup for future experiments with such liquids.

Data availability statement

All data that support the findings of this study are included within the article.

Acknowledgment

This work was supported by the Czech Science Foundation EXPRO Project 21-26601X. We thank A Milosavljević and Ch Nicolas from Synchrotron Soleil, France, for numerous discussions and for the possibility of hands-on experience with liquid microjets. The missions to Soleil were supported by the MEYS Grant No. LTC20067.

ORCID iDs

Pamir Nag https://orcid.org/0000-0002-1530-6104
Miloš Ranković https://orcid.org/0000-0003-1317-0132
Leo Sala https://orcid.org/0000-0003-1091-4386
Jaroslav Kočišek https://orcid.org/0000-0002-6071-2144

References

[1] Fabrikant I I, Eden S, Mason N J and Fedor J 2017 *Adv. At. Mol. Opt. Phys.* **66** 545–657
[2] Fárník M, Fedor J, Kočišek J, Lengyel J, Pluhařová E, Poterya V and Pysanenko A 2021 *Phys. Chem. Chem. Phys.* **23** 3195–213
[3] Böhler E, Warneke J and Swiderek P 2013 *Chem. Soc. Rev.* **42** 9219–31
[4] Boudaïffa B, Cloutier P, Hunting D, Huels M A and Sanche L 2000 *Science* **287** 1658–60
[5] Faubel M and Steiner B 1994 *Photoelectron Spectroscopy at Liquid Water Surfaces* (Springer) pp 517–23
[6] Faubel M, Schlemmer S and Toennies J P 1988 *Z. Phys.* D **10** 269–77
[7] Faubel M and Kisters T 1989 *Nature* **339** 527–9
[8] Ekimova M, Quevedo W, Faubel M, Wernet P and Nibbering E T J 2015 *Struct. Dyn.* **2** 054301
[9] Faubel M, Steiner B and Toennies J P 1997 *J. Chem. Phys.* **106** 9013–31
[10] Winter B and Faubel M 2006 *Chem. Rev.* **106** 1176–211
[11] Faust J A and Nathanson G M 2016 *Chem. Soc. Rev.* **45** 3609–20
[12] Nesbitt D J, Zolot A M, Roscioli J R and Ryazanov M 2023 *Acc. Chem. Res.* **56** 700–11
[13] Nomura S, Tsuchida H, Furuya R, Miyahara K, Majima T and Itoh A 2015 *Nucl. Instrum. Methods Phys. Res.* B **365** 611–5
[14] Koralek J D *et al* 2018 *Nat. Commun.* **9** 1353
[15] Luu T T, Yin Z, Jain A, Gaumnitz T, Pertot Y, Ma J and Wörner H J 2018 *Nat. Commun.* **9** 3723
[16] Schewe H C, Credidio B, Ghrist A M, Malerz S, Ozga C, Knie A, Haak H, Meijer G, Winter B and Osterwalder A 2022 *J. Am. Chem. Soc.* **144** 7790–5
[17] Lee C, Pohl M N, Ramphal I A, Yang W, Winter B, Abel B and Neumark D M 2022 *J. Phys. Chem.* A **126** 3373–83
[18] Chen L, Chen Z, Li Z, Hu J and Tian S X 2018 *Rev. Sci. Instrum.* **89** 103102
[19] Chen Z Li Z, Hu J and Tian S X 2022 *Acc. Chem. Res.* **55** 3071–9
[20] Muccignat D L, Stokes P W, Cocks D G, Gascooke J R, Jones D B, Brunger M J and White R D 2022 *Int. J. Mol. Sci.* **23** 3354
[21] Itikawa Y and Mason N 2005 *J. Phys. Chem. Ref. Data* **34** 1–22
[22] Song M Y, Cho H, Karwasz G P, Kokoouline V, Nakamura Y, Tennyson J, Faure A, Mason N J and Itikawa Y 2021 *J. Phys. Chem. Ref. Data* **50** 023103
[23] Karwasz G, Brusa R and Zecca A 2003 *Interactions of Photons and Electrons with Molecules* (Springer) pp 6001–51
[24] Faubel M, Schlemmer S and Toennies J 1988 *Z. Phys.* D **10** 269–77
[25] Milosavljević A R, Madžunkov S, Šević D, Čadež I and Marinković B P 2006 *J. Phys. B: At. Mol. Opt. Phys.* **39** 609
[26] Allan M 1995 *J. Phys. B: At. Mol. Opt. Phys.* **28** 5163
[27] Stanton J, Taucher-Schoiz G, Schneider M, Heilmann J and Kraft G 1993 *Radiat. Environ. Biophys.* **32** 21–32
[28] Hicks M and Gebicki J M 1986 *FEBS Lett.* **199** 3563
[29] Roush A E, Riaz M, Misra S K, Weinberger S R and Sharp J S 2020 *J. Am. Soc. Mass Spectrom.* **31** 169–72
[30] Gutmann B, Cantillo D and Kappe C O 2015 *Angew. Chem., Int. Ed.* **54** 6688–728
[31] Cambié D, Bottecchia C, Straathof N J W, Hessel V and Noël T 2016 *Chem. Rev.* **116** 10276–341
[32] Klaiman S and Cederbaum L S 2015 *Angew. Chem., Int. Ed.* **54** 10470–3
[33] König B 2019 *Science of Synthesis: Photocatalysis in Organic Synthesis* (Thieme)